JTTEE5 19:873–878
DOI: 10.1007/s11666-010-9496-x
1059-9630/$19.00 © ASM International

Plasma Sprayed Dense MgO-Y_2O_3 Nanocomposite Coatings Using Sol-Gel Combustion Synthesized Powder

Jiwen Wang, Eric H. Jordan, and Maurice Gell

(Submitted July 13, 2009; in revised form March 8, 2010)

MgO-Y_2O_3 nanostructured composite powder (volume ratio of 50:50) was synthesized by a sol-gel combustion process which generated crystal sizes in the 10-20 nm range. The MgO-Y_2O_3 nanopowder was plasma sprayed using a conventional, DC arc plasma spray system. X-ray diffraction analysis shows that the as-sprayed MgO-Y_2O_3 coating is composed of cubic MgO and Y_2O_3 phases and has ~95% density. Microstructure characterization by SEM reveals that the as-sprayed coating has fine grain sizes of 100-300 nm as a result of rapid solidification. The hardness of the coating, 7.5 ± 0.6 GPa, is higher than that of coarse-grained, dense MgO, and Y_2O_3 ceramics. This approach demonstrates the potential of plasma spray processes for making thick, dense MgO-Y_2O_3 nanocomposite performs for applications as durable, infrared windows.

Keywords air plasma spray, magnesia, nanocomposite, plasma spray coatings, yttria

1. Introduction

Plasma sprayed nanostructured and nanocomposite coatings have exhibited promising mechanical properties, such as hardness, strength, and wear resistance over conventional micrograined coatings and therefore have gained considerable attention (Ref 1-3). Different plasma spray technologies have been used to achieve nanostructured and nanocomposite coatings, which include air plasma spray (APS) (Ref 1-5), suspension plasma spray (SPS) (Ref 6-10), and solution precursor plasma spray (SPPS) (Ref 11, 12). In APS, nanoparticles cannot be thermally sprayed using conventional powder feeders. The powders must be agglomerated to sprayable sizes using a spray dry process (Ref 1, 2).

Recently, MgO-Y_2O_3 nanocomposites were reported to have excellent mid-infrared transparency and improved mechanical properties for use as infrared window materials (Ref 13). In Ref 13, the powder was made by a combustion spray pyrolysis process and consolidated to bulk structures, using a series of powder classification, purification, and sintering techniques. This study seeks to directly deposit a nanocomposite preform, with fewer consolidation steps, using APS. Limiting the phase domain size to the nanoscale is important to minimize the light scattering at the two-phase grain boundaries and to further improve the mechanical properties of MgO-Y_2O_3 nanocomposite ceramics. The rapid solidification characteristics of plasma spray may be a useful tool to achieve such required nanostructures. In order to produce small phase domains in the end point material and to have the lower melting temperature corresponding to the composite rather than the higher melting point of the individual constituents the powder must have small phase domains. In thermal spray, the time at melting temperature is less than 1 ms and only very small scale inhomogeneity can be removed during heating.

In this study, a two-phase MgO-Y_2O_3 nanopowder with volume ratio of 50:50 was synthesized by a sol-gel combustion process and micrometer-size agglomerated powder was deposited by APS forming dense thick coatings. Sprayable powder was created without the use of a spray dry process, an expensive process requiring significant development work for each new powder. The phase composition, surface morphology, microstructure, and hardness of the as-sprayed coatings were investigated.

Jiwen Wang, Department of Chemical, Materials and Biomolecular Engineering, Institute of Materials Science, University of Connecticut, Storrs, CT and Navy Research Laboratory, Code 6364, Washington, DC 20375; **Eric H. Jordan**, Department of Mechanical Engineering, Institute of Materials Science, University of Connecticut, Storrs, CT; and **Maurice Gell**, Department of Chemical, Materials and Biomolecular Engineering, Institute of Materials Science, University of Connecticut, Storrs, CT. Contact e-mails: jordan@engr.uconn.edu and wangjiwen@gmail.com.

2. Experimental Procedure

2.1 Powder Synthesis

Magnesium acetate ($(CH_3COO)_2Mg \cdot 4H_2O$, >99%, Alfa Aesar), yttrium nitrate ($Y(NO_3)_3 \cdot 6H_2O$, >99.9%, Alfa Aesar) were used as starting chemicals. The above chemicals were first dissolved in deionized water based on the volume fraction ratio of 50:50 of the oxides. After

mixing for 10 h, the solution was dried in an oven at 200 °C, during which a white gel formed. The dried gel was then heated in an oven to 600 °C with a heating rate of 20 °C/min. During the heating process, rapid combustion occurred and voluminous fluffy powder was formed. After de-carbonization at 600 °C for 2 h, white powder was produced and collected. A ball-milling process was applied to the collected powder to break down large agglomerates into micrometer-sized particles. ZrO_2 balls were used as ball-milling media. Single-phase nanopowders are available, but mixed phase powders with small homogeneously mixed phases are not readily available.

2.2 Plasma Spray

The MgO-Y_2O_3 nanocomposite coatings were deposited using a direct current plasma torch (Metco 9 MB, Sulzer Metco, Westbury, NY) attached to a six-axis robotic arm. Argon and hydrogen were used as the primary and secondary plasma gases, respectively. Argon gas flow rate was 80 SCFH. Current and voltage of the plasma arc used were 600 A and 60 V, resulting in the plasma power of 36 kW. The powder was fed using a conventional fluidized bed feeder (Metco 9MP, Sulzer Metco, Westbury, NY) with a feed rate of ~10 g/min. The coatings were deposited on grit-blasted (Al_2O_3 grit of #30 mesh size) 304 stainless steel disk substrates (25 mm diameter, 3 mm thickness). The spraying distances were 44.5 mm. The substrate temperature was measured by a thermocouple right after the preheating and the coating deposition. The number of coating passes deposited on the substrates was 180 with a deposition rate of ~18 μm/pass and a deposition efficiency of ~30%. The robotic arm traverse speed was 1000 mm/s.

2.3 Characterization

Differential thermal analysis (DTA) and thermal gravimetric (TG) analysis were performed simultaneously on dried precursor using a SDT-Q6000 thermal analyzer (TA Inc., New Castle, DE) with flowing air by heating the sample from room temperature to 1000 °C at a heating rate of 10 °C/min. The crystalline phase composition of the as-synthesized powder and plasma sprayed coatings was determined using x-ray diffraction (XRD) (Cu Kα radiation, D8, Bruker AXS, Karlsruhe, Germany). A JEOL HRTEM (JEOL 2010, Tokyo, Japan) was used to characterize the crystalline size of the nanopowder. An environmental scanning electron microscope (ESEM 2020, Philips Electron Optics, Eindhoven, the Netherlands) and a JEOL JSM-6335F field emission scanning electron microscope (FESEM, Tokyo, Japan) were used to characterize the morphology of the powder agglomerates and the coating microstructure. Coating porosity was measured on the polished cross sections by image analysis. Macroscopic photos of the as-sprayed coatings were taken by a Sony P5 digital camera (Sony, Tokyo, Japan). The Vickers hardness (HV) was measured on the polished cross-sections with a 2.94 N normal load and a dwell time of 15 s. The hardness value is the average of 10 measurements.

3. Experimental Results and Discussion

3.1 TG-DTA Analysis of Precursor Gel

The typical TG-DTA curves of the 200 °C dried MgO-Y_2O_3 precursor as a function of temperature at a heating rate of 10 °C/min are shown in Fig. 1. The sample weight decreases continuously with the increasing of temperature from ~25 to 1000 °C, and the total weight loss is about 67%. There were two exothermic peaks at 326 and 419 °C, which can be ascribed to the pyrolysis of the precursor and is coincident with the abrupt weight loss in this temperature range. The TG curve shows that after 600 °C, the pyrolysis process is complete and the minor weight loss (~2%) thereafter, is attributed to de-carbonization.

3.2 XRD, SEM, and HRTEM Analysis of MgO-Y_2O_3 Nanopowder

XRD analysis (Fig. 2) shows that the as-synthesized MgO-Y_2O_3 nanocomposite powder is composed of phase-pure cubic MgO (PDF card No. 04-0829) and Y_2O_3 (PDF card No. 05-0574). The average grain size calculated from the peak broadening effect using Scherrer's formula is ~15 nm. The particle size and morphology of the as-synthesized and ball-milled powder are shown in Fig. 3(a) and (b), respectively. The as-synthesized composite powder agglomerates have a particle size distribution

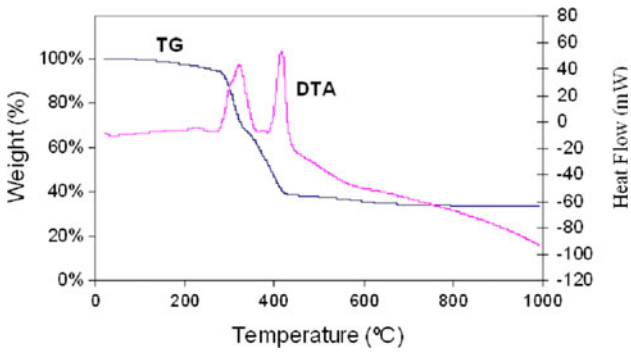

Fig. 1 Thermal gravimetric-differential thermal analysis curves of dried MgO-Y_2O_3 precursor at a heating rate of 10 °C/min

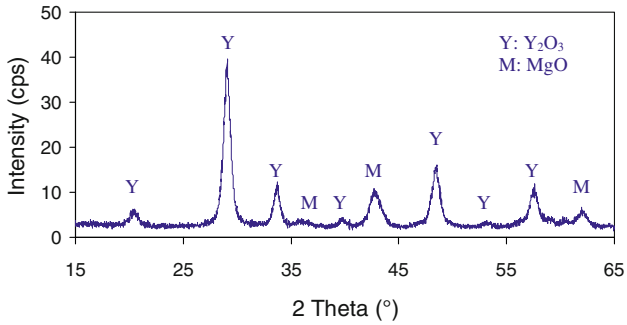

Fig. 2 X-ray diffraction pattern of as-synthesized MgO-Y_2O_3 nanopowder

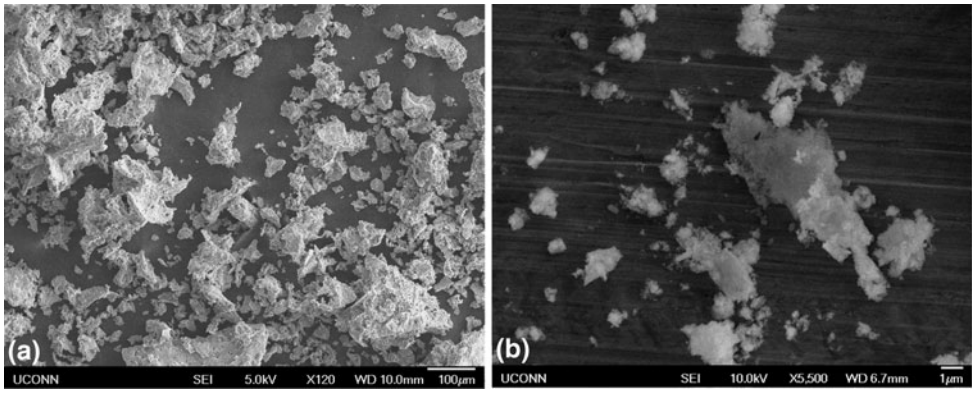

Fig. 3 Morphology of MgO-Y_2O_3 nanopowder: (a) as-synthesized and (b) ball-milled

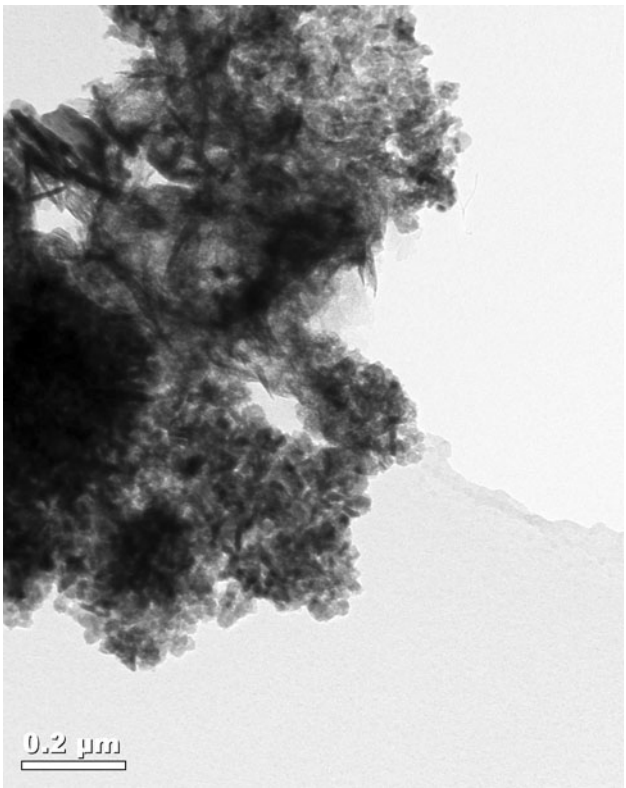

Fig. 4 Bright field TEM image of as-synthesized MgO-Y_2O_3 nanopowder

of 10-100 μm with an average particle size of ~50 μm (Fig. 3a). After ball-milling, the average particle size was reduced to ~3 μm (Fig. 3b) with a size distribution of 1-10 μm. HRTEM analysis (Fig. 4) shows that the ball-milled MgO-Y_2O_3 nanopowder has micron-sized agglomerates composed of small MgO and Y_2O_3 crystals between 10 and 20 nm, which is consistent with the XRD results (Fig. 2). Nanosized fine powders cannot be used for thermal spray due to the high surface force to inertia force ratio that prevents traditional fluidized powder feeding and also due to the fact of high drag force to inertia force

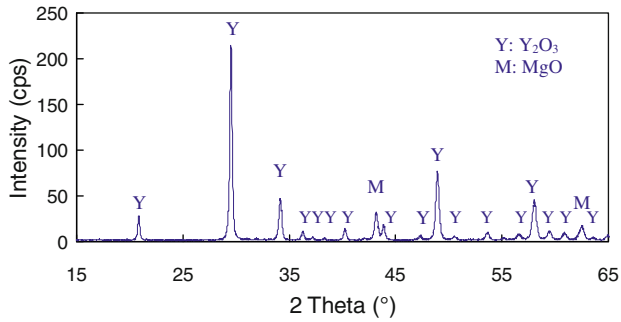

Fig. 5 X-ray diffraction pattern of as-sprayed MgO-Y_2O_3 coating

ratio that prevents small particles from penetrating the stationary gas layer at the substrate. In this study, with micron-sized agglomeration, MgO-Y_2O_3 nanopowder was fed directly into the plasma jet using a commercial powder feeder and successfully deposited on substrates.

3.3 Plasma Sprayed MgO-Y_2O_3 Nanocomposite Coatings

During the APS process, five passes of plasma jet preheating on the substrate and 180 coating passes were carried out and the substrate temperatures measured by a thermocouple right after the preheating and coating deposition were ~200 and 700 °C, respectively. Figure 5 shows a XRD pattern of the as-sprayed coating. The coating consists of cubic MgO and Y_2O_3 phases, as was similarly determined for the as-synthesized powders. Figure 6(a) is a macroscopic photo of the MgO-Y_2O_3 coating (after surface grinding) on a stainless steel substrate after 180 thermal spray passes. The coating has a thickness of 3.2 mm and has good bonding with the substrate. Figure 6(b) is the representative surface morphology of the as-sprayed MgO-Y_2O_3 coatings. The coating surface is composed of fine splats (2-15 μm), indicating that the MgO-Y_2O_3 powders were fully melted in the plasma plume and solidified during coating deposition. The splat size is equal to the size of the MgO-Y_2O_3 agglomerates after ball-milling (Fig. 3b), and is significantly

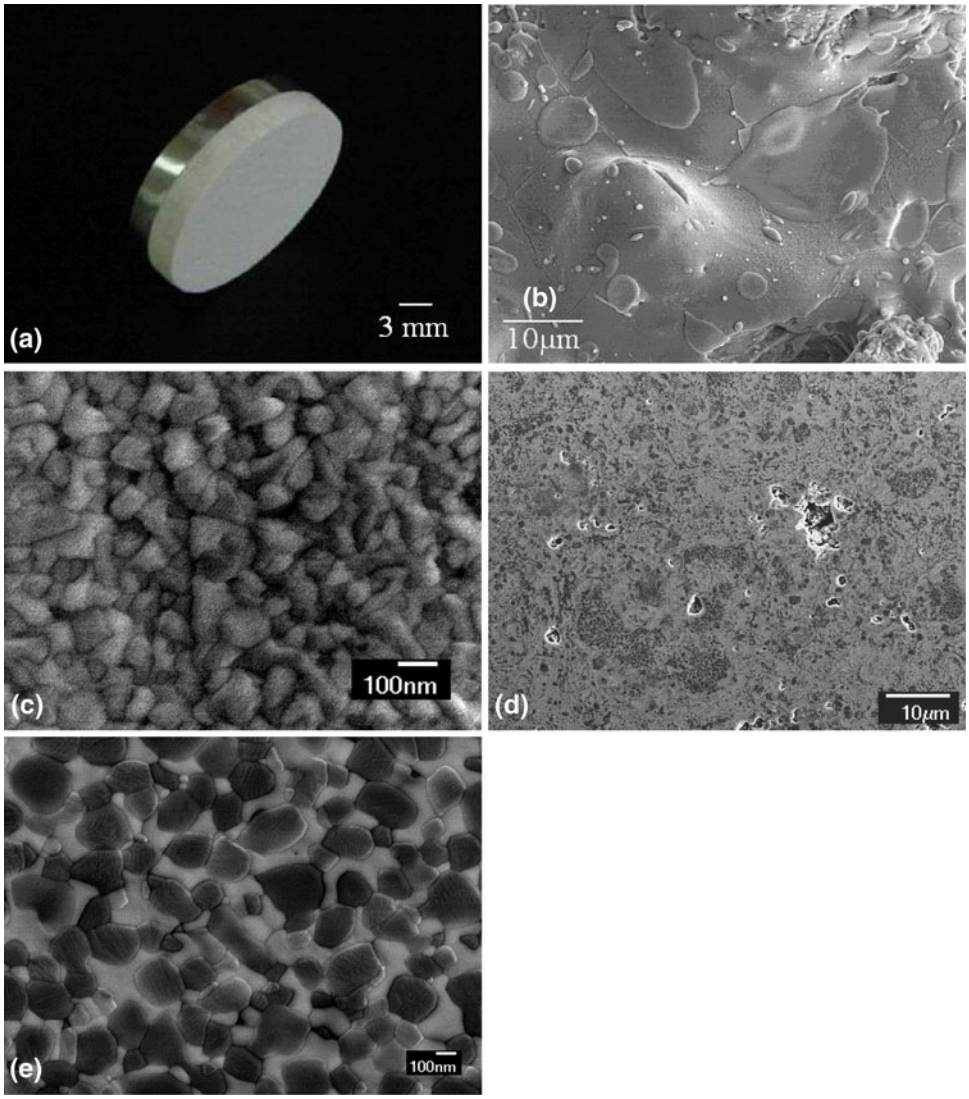

Fig. 6 (a) macroscopic photo of the as-sprayed coating, (b) representative surface morphology of the coating, (c) high magnification SEM image of the coating surface, (d) typical SEM image of polished cross-sections, and (e) high magnification SEM image of a polished cross-section

smaller than conventional APS splats (~100 μm). Fully melted powder and fine splats are critical to producing dense ceramic coatings (Ref 14). Figure 6(c) shows a back-scattered high magnification SEM micrograph of the coating surface. MgO and Y_2O_3 nanograins are present, with an average grain size of about 100 nm. The nanometer grain size results from the small crystal size of the nanopowders and rapid solidification at the coating surface. A typical microstructure of the polished cross section of the MgO-Y_2O_3 coating is shown in Fig. 6(d). The coating is ~95% dense, with micrometer-sized pores ranging from 1 to 10 μm. The size and distribution of the pores are in agreement with that of the MgO-Y_2O_3 powder agglomerates after ball-milling (Fig. 3b). There are no obvious splat boundaries or layered structures observed in the coatings. Occasional phase distribution fluctuations on the micrometer scale were noticed. These may due to the inhomogeneous distribution of phases in the original powders. A high-magnification SEM image of the cross section (Fig. 6e) shows interpenetrated and homogeneously distributed MgO (darker phase) and Y_2O_3 (brighter phase) nanograins and domains ranging from 100 to 300 nm. The increase of MgO and Y_2O_3 grain sizes, compared with that of the coating surface (Fig. 6c), is due to the accumulated heat treatment from the plasma plume. The Vickers hardness of the coatings is 7.5 ± 0.6 GPa, with individual hardness readings ranging from 6.5 to 8.1 GPa.

It is well-known that the heat transfer rate of particles in a plasma plume increases proportionally with surface area. In air plasma spraying, the time for powder melting is on the order of 1 ms and hence large MgO-Y_2O_3 phase domains, which may begin melting at the eutectic temperature (2110 °C) would not have time to melt as a eutectic phase and would therefore have to melt at two constituent melting points, which is 2825 °C for MgO and

2410 °C for Y_2O_3. In this study, MgO-Y_2O_3 nanopowders have a large surface area and short diffusion paths between MgO and Y_2O_3 nanodomains. This allows rapid melting of the nanopowders with the eutectic composition. Rapidly melted eutectic MgO-Y_2O_3 domains may surround the remaining MgO domains to inhibit them from sublimating, which is considered to be the main problem for the plasma spray of MgO single-phase powder (Ref 15). The fine nanocrystalline microstructure of the coatings is attributed to the fine crystal size of the nanopowders and rapid solidification of the deposited splats. It may also be attributed to grain growth inhibition by a dual-phase microstructure (Ref 16).

The hardness of the MgO-Y_2O_3 nanocomposite coatings (with an average Vickers hardness of 7.5 GPa and a maximum value of 8.1 GPa) is significantly higher than that of MgO and Y_2O_3 coarse-grained, dense ceramics (Vickers hardness typically between 5 and 7 GPa) (Ref 17). It has been demonstrated that the mechanical strength and thermal shock resistance of ceramics can be increased with decreasing grain size and normal Hall-Petch relationships were found in some ceramic systems (Ref 18-21). Rice et al. (Ref 17) showed that the hardness of Y_2O_3 increases from ~7 to ~9 GPa with the decrease of grain size from ~100 to ~1 μm. A similar trend was also found in MgO dense ceramics when the grain size is smaller than ~25 μm (an increase of hardness from ~5 to ~9 GPa when the grain size decreases from ~25 to ~1 μm). The hardening of MgO-Y_2O_3 nanocomposite coatings is considered due to the normal Hall-Petch effects from small grain sizes (Ref 22, 23). Nanocrystalline ceramics are highly desirable for improving the mechanical properties (Ref 24). Due to its rapid solidification characteristics, plasma spray is able to make nanocrystalline coatings without using complicated ceramic powder processing and sintering steps. There is the potential to further increase the hardness of MgO-Y_2O_3 coatings by optimizing the thermal spray conditions to reduce the porosity (also critical for mid-infrared transparency), to further decrease grain size, and to add ternary oxides.

4. Conclusions

MgO-Y_2O_3 composite nanopowder was synthesized by a sol-gel combustion process, which created 10-20 nm MgO and Y_2O_3 crystals. The MgO-Y_2O_3 nanopowder feedstock was successfully deposited on substrates by APS without the use of spray dry agglomeration. XRD analysis shows that the coating is composed of cubic MgO and Y_2O_3 phases. As-sprayed dense MgO-Y_2O_3 nanocomposite coatings are mainly composed of fine splats (2-15 μm) with MgO and Y_2O_3 grain sizes of 100-300 nm. The hardness of the coatings is 7.5 ± 0.6 GPa, which is significantly higher than that of coarse-grained MgO and Y_2O_3 dense ceramics. This plasma spray approach demonstrates the potential of fabricating MgO-Y_2O_3 nanocomposite dense preforms for possible applications as durable mid-infrared transparent windows.

Acknowledgments

This work is supported by a sub-contract from Raytheon Corporation, from a prime contract funded by DARPA/ONR. We also appreciate the characterization support of Dr. Lichun Zhang and Mr. Chigozie Muoto.

References

1. E.H. Jordan, M. Gell, Y.H. Sohn, D. Goberman, L. Shaw, S. Jiang, M. Wang, T.D. Xiao, Y. Wang, and P.R. Strutt, Fabrication and Evaluation of Plasma Sprayed Nanostructured Alumina-Titania Coatings with Superior Properties, *Mater. Sci. Eng. A Struct. Mater. Prop. Microstruct. Process.*, 2001, **301**(1), p 80-89
2. L.L. Shaw, D. Goberman, R.M. Ren, M. Gell, S. Jiang, Y. Wang, T.D. Xiao, and P.R. Strutt, The Dependency of Microstructure and Properties of Nano-structured Coatings on Plasma Spray Conditions, *Surf. Coat. Technol.*, 2000, **130**(1), p 1-8
3. H. Chen, C.X. Ding, P.Y. Zhang, P.Q. La, and S.W. Lee, Wear of Plasma-Sprayed Nanostructured Zirconia Coatings Against Stainless Steel Under Distilled-Water Conditions, *Surf. Coat. Technol.*, 2003, **173**(2-3), p 144-149
4. R.S. Lima and B.R. Marple, Thermal Spray Coatings Engineered From Nanostructured Ceramic Agglomerated Powders for Structural. Thermal Barrier and Biomedical Applications: A Review, *J. Therm. Spray Technol.*, 2007, **16**(1), p 40-63
5. R.S. Lima and B.R. Marple, APS to HVOF Spraying of Conventional and Nanostructured Titania Feedstock Powders: A Study on the Enhancement of the Mechanical Properties, *Surf. Coat. Technol.*, 2006, **200**(11), p 3428-3437
6. P. Fauchais, V. Rat, U. Delbos, J.F. Coudert, T. Chartier, and L. Bianchi, Understanding of Suspension DC Plasma Spraying of Finely Structured Coatings for SOFC, *IEEE Trans. Plasma Sci.*, 2005, **33**(2), p 920-930
7. J.O. Berghaus, B. Marple, and C. Moreau, Suspension Plasma Spraying of Nanostructured WC-12Co Coatings, *J. Therm. Spray Technol.*, 2006, **15**(4), p 676-681
8. J.O. Berghaus, J.G. Legoux, C. Moreau, F. Tarasi, and T. Chraska, Mechanical and Thermal Transport Properties of Suspension Thermal-Sprayed Alumina-Zirconia Composite Coatings, *J. Therm. Spray Technol.*, 2008, **17**(1), p 91-104
9. H. Kassner, R. Siegert, D. Hathiramani, R. Vassen, and D. Stoever, Application of Suspension Plasma Spraying (SPS) for Manufacture of Ceramic Coatings, *J. Therm. Spray Technol.*, 2008, **17**(1), p 115-123
10. F.L. Toma, G. Bertrand, D. Klein, C. Coddet, and C. Meunier, Nanostructured Photocatalytic Titania Coatings Formed by Suspension Plasma Spraying, *J. Therm. Spray Technol.*, 2006, **15**(4), p 587-592
11. D. Chen, E.H. Jordan, M. Gell, and X.Q. Ma, Dense Alumina-Zirconia Coatings Using the Solution Precursor Plasma Spray Process, *J. Am. Ceram. Soc.*, 2008, **91**(2), p 359-365
12. M. Gell, L.D. Xie, X.Q. Ma, E.H. Jordan, and N.P. Padture, Highly Durable Thermal Barrier Coatings Made by the Solution Precursor Plasma Spray Process, *Surf. Coat. Technol.*, 2004, **177-178**, p 97-102
13. T. Stefanik, R. Gentilman, and P. Hogan, Nanocomposite Optical Ceramics for Infrared Windows and Domes, *Proc. SPIE*, 2007, **6545**, p 65450A1-65450A5
14. D. Chen, E.H. Jordan, M. Gell, and X.Q. Ma, Dense TiO_2 Coating Using the Solution Precursor Plasma Spray Process, *J. Am. Ceram. Soc.*, 2008, **91**(3), p 865-872
15. O. Fukumasa, R. Tagashira, K. Tachino, and H. Mukunoki, Spraying of MgO Films with a Well-Controlled Plasma Jet, *Surf. Coat. Technol.*, 2003, **169-170**, p 579-582
16. D. Joanthan, M.P.H. French, M.C. Helen, and G.A. Miller, Coarsening Resistant Dual-Phase Interpenetrating Microstructures, *J. Am. Ceram. Soc.*, 1990, **73**(8), p 2508-2510

17. R.W. Rice, C.C. Wu, and F. Borchelt, Hardness-Grain-Size Relations in Ceramics, *J. Am. Ceram. Soc.*, 1994, **77**(10), p 2539-2553
18. R. Vaßen and D. Stöver, Processing and Properties of Nanophase Non-Oxide Ceramics, *Mater. Sci. Eng. A Struct. Mater. Prop. Microstruct. Process.*, 2001, **301**, p 59-68
19. A. Bellosi, D. Sciti, and S. Guicciardi, Synergy and Competition in Nano- and Micro-design of Structural Ceramics, *J. Euro. Ceram. Soc.*, 2004, **24**, p 3295-3302
20. Z. Shen, M. Johnsson, Z. Zhao, and M. Nygren, Spark Plasma Sintering of Alumina, *J. Am. Ceram. Soc.*, 2002, **85**(8), p 1921-1927
21. N. Bamba, Y.H. Choa, and K. Niihara, Fabrication and Mechanical Properties of Nanosized SiC Particulate Reinforced Yttria Stabilized Zirconia Composites, *Nonostruct. Mater.*, 1997, **9**, p 497-500
22. J.C.M. Li, Petch Relation and Grain Boundary Sources, *Trans. AIME*, 1963, **227**, p 239-247
23. M.A. Meyers and K.K. Chawla, *Mechanical Metallurgy: Principles and Applications*, Prentice-Hall. Inc, Englewood Cliffs, NJ, 1984
24. S.C. Tjong and H. Chen, Nanocrystalline Materials and Coatings, *Mater. Sci. Eng. R*, 2004, **45**(1-2), p 1-88